Draft version January 25, 2010
Preprint typeset using LaTeX style emulateapj v. 11/10/09

arXiv:0905.1115v2 [astro-ph.HE] 25 Jan 2010

MODELING THE EXTRAGALACTIC BACKGROUND LIGHT FROM STARS AND DUST

Justin D. Finke,[1] Soebur Razzaque[1] and Charles D. Dermer
U.S. Naval Research Laboratory, Code 7653, 4555 Overlook Ave SW, Washington, DC 20375-5352
[1]NRL/NRC Research Associate

Draft version January 25, 2010

ABSTRACT

The extragalactic background light (EBL) from the far infrared through the visible and extending into the ultraviolet is thought to be dominated by starlight, either through direct emission or through absorption and reradiation by dust. This is the most important energy range for absorbing γ-rays from distant sources such as blazars and gamma-ray bursts and producing electron-positron pairs. In previous work we presented EBL models in the optical through ultraviolet by consistently taking into account the star formation rate (SFR), initial mass function (IMF) and dust extinction, and treating stars on the main sequence as blackbodies. This technique is extended to include post-main sequence stars and reprocessing of starlight by dust. In our simple model, the total energy absorbed by dust is assumed to be re-emitted as three blackbodies in the infrared, one at 40 K representing warm, large dust grains, one at 70 K representing hot, small dust grains, and one at 450 K representing polycyclic aromatic hydrocarbons. We find our best fit model combining the Hopkins and Beacom SFR using the Cole et al. parameterization with the Baldry and Glazebrook IMF agrees with available luminosity density data at a variety of redshifts. Our resulting EBL energy density is quite close to the lower limits from galaxy counts and in some cases below the lower limits, and agrees fairly well with other recent EBL models shortward of about 5 μm. Deabsorbing TeV γ-ray spectra of various blazars with our EBL model gives results consistent with simple shock acceleration theory. We also find that the universe should be optically thin to γ-rays with energies less than 20 GeV.

Subject headings: galaxies: active — diffuse radiation — gamma rays: observations — stars: luminosity function, mass function — stars: formation

1. INTRODUCTION

The extragalactic background light (EBL) from $\sim 10^{-3}$ – 10 eV (~ 0.1 – $1000\,\mu$m) is thought to be dominated by starlight, either through direct emission, or through absorption and reradiation by dust. This is the most important energy range for photons with energy E_1(TeV) interacting with long-wavelength photons with and absorbing γ-rays from distant sources, with the threshold $\gamma\gamma$ condition implying that

$$E_1(TeV) = \frac{0.26}{(1+z)\ E_{EBL}(eV)}\ .$$

The EBL is also an important target radiation field for energy-loss and/or photodisintegration of the highest energy cosmic ray protons and ions (e.g., Puget et al. 1976), which results in a source of high-energy neutrinos (e.g. Stanev 2004). Direct measurement of the EBL is difficult (see Hauser & Dwek 2001, for a review) due to contamination by foreground zodiacal and Galactic light. Galaxy counts may also be used to estimate the EBL, but the unknown number of unresolved sources results in a lower limit. The general picture is a component peaking at around 1 μm from direct starlight emission and one peaking at ~ 100 μm from re-emission of absorbed starlight by dust. Due to different modeling approaches and uncertainties in underlying model parameters, the intensity and shape of the EBL spectrum remains controversial.

A wide range of EBL models have been developed. One class of models approaches the problem by using IR data from local galaxies and extrapolating their evolution to higher redshifts and shorter wavelengths (e.g., Malkan & Stecker 1998, 2001; Stecker et al. 2006). Another class of models uses semi-analytic merger-tree models of galaxy formation to determine the star formation history of the universe for a forward-evolution calculation (Primack et al. 2001, 2005, 2008; Gilmore et al. 2008, 2009). The class of models considered here focuses on the primary energy source of the emission, namely the stars. In such models, one integrates over star formation rates and stellar properties (e.g. Salamon & Stecker 1998; Dwek et al. 1998; Kneiske et al. 2002, 2004). Alternatively, luminosity density data (Franceschini et al. 2008) is used to estimate the EBL energy density and its evolution with time. Since the EBL absorbs very high energy (VHE; ≈ 0.1 – 100 TeV) γ-rays from blazars, one can use this mechanism to put upper limits on the EBL energy density (e.g., Stecker & de Jager 1993; Stanev & Franceschini 1998; Aharonian et al. 2006; Mazin & Raue 2007; Finke & Razzaque 2009). Disagreement about the intrinsic γ-ray spectra of blazars (e.g., Stecker et al. 2007; Böttcher et al. 2008) has resulted, however, in a lack of consensus about the meaning of these upper limits. Detection of a 33 GeV photon from GRB 090902B (Abdo et al. 2009a) and a 13 GeV photon from GRB 080916C (Abdo et al. 2009b) with the Large Area Telescope (LAT) onboard the *Fermi* Gamma Ray Space Telescope are used to test different EBL models, which may be a promising new way to constrain the EBL.

We (Razzaque, Dermer, & Finke 2009, hereafter RDF09) recently developed models for starlight luminosity density and EBL intensity by assuming that stars

justin.finke@nrl.navy.mil

are blackbodies, and integrating over stellar properties on the main sequence. Here we extend the model of RDF09 to stars that have evolved off the main sequence and include re-emission of absorbed starlight by dust, noting that the models of RDF09 remain valid for the $\gtrsim$ 1 eV range. In § 2, analytic expressions for the radiation from stars and re-emission by dust are presented. Numerical calculations of the luminosity density and EBL energy density are presented in § 3. We explore the effects of our EBL model on absorption of distant γ-rays (§ 4) and conclude with a discussion on our results and future research (§ 5).

2. FORMALISM

We briefly describe the RDF09 model for background starlight and our recent improvements which include the emission from post-main sequence stars and dust. Integrating over star formation in this manner is similar to several other models (e.g. Salamon & Stecker 1998; Dwek et al. 1998; Kneiske et al. 2002, 2004).

2.1. *Direct Starlight Emission*

Stars with dimensionless mass $m = M/M_\odot$ and age $t_\star$ are assumed to emit as blackbodies. The photon density of a blackbody is given by

$$n_\star(\epsilon; m, \Theta) = \frac{dN}{d\epsilon dV} = \frac{8\pi}{\lambda_C^3} \frac{\epsilon^2}{\exp[\epsilon/\Theta] - 1} \qquad (1)$$

where $\epsilon = h\nu/m_e c^2$ is the dimensionless photon energy, $\lambda_C = h/m_e c \approx 2.42 \times 10^{-10}$ cm is the Compton wavelength, and $\Theta = k_B T/m_e c^2$ is the dimensionless effective temperature. The total number of photons emitted per unit energy per unit time from a star of radius $R(m, t_\star)$ and effective stellar temperature $\Theta(m, t_\star)$ is

$$\dot{N}_\star(\epsilon; m, t_\star) = \frac{dN}{d\epsilon dt} = \pi R(m, t_\star)^2 c \; n_\star(\epsilon; \Theta(m, t_\star)) \; . \quad (2)$$

To determine the luminosities and radii of the stars, $L(m, t_\star)$ and $R(m, t_\star)$, respectively, as well as the time stars spend on various portions of the Hertzsprung-Russell diagram, we used the stellar formulae from the appendix of Eggleton et al. (1989). These formulae approximate the stellar parameters along the main sequence, the Hertzsprung gap, the giant branch, the horizontal branch, the asymptotic giant branch, and the white dwarf phase for stars of solar metalicity. Thus, we assume all stars emitting since star formation began have solar metalicity. Note that eqn. (A15) of Eggleton et al. (1989), which describes the luminosity of the base of the giant branch, should be

$$L_{BGB} = \frac{2.15M^2 + 0.22M^5}{1 + 1.4 \times 10^{-2} M^2 + 5 \times 10^{-6} M^4}$$

(Eggleton et al. 1990). Also, eqn. (A22) of Eggleton et al. (1989), which describes the time a star spends burning Helium, should be

$$t_{He} = \frac{t_{MS} L_0}{L_{He}(M^{0.42} + 0.8)}$$

(C. Tout and P. Eggleton, private communication). We modify eqn. (A27) of Eggleton et al. (1989), which describes the luminosity of a white dwarf in our calculations, so that it reads

$$L = \frac{40}{(t - t_{WD} + 0.1)^{1.4}}$$

in order to avoid a singularity when $t = t_{WD}$ (Hurley et al. 2000). In the above corrections to Eggleton et al. (1989), we use their notation, so that M is the star's mass in units of $M_\odot$, L_{BGB} and L_0 are in units of $L_\odot$, and t, t_{He}, t_{MS}, and t_{WD} are in units of Myr.

Once a star's luminosity and radius have been determined, its temperature can be found by

$$\Theta(m, t_\star) = \frac{k_B T_\odot}{m_e c^2} \left(\frac{L(m, t_\star)}{L_\odot} \right)^{1/4} \sqrt{\frac{R_\odot}{R(m, t_\star)}} \qquad (3)$$

where $T_\odot = 5777$ K is the effective solar temperature, $L_\odot = 3.846 \times 10^{33}$ erg s^{-1} is the solar luminosity, and $R_\odot = 6.96 \times 10^{10}$ cm is the solar radius.

We will use unprimed symbols to refer to quantities measured in the frame comoving with the Hubble flow, and primed or double primed quantities to refer to quantities in the proper frame of a galaxy at some redshift z. Observations made from the solar system, which has a small peculiar velocity with respect to the Hubble flow, are essentially in the comoving frame. The comoving luminosity density (i.e., the luminosity per unit comoving volume, or the emissivity) of the universe as a function of comoving energy ϵ at a certain redshift z (in units of, e.g., W Mpc^{-3}) can be found from

$$\epsilon \, j^{stars}(\epsilon; z) = m_e c^2 \epsilon^2 \frac{dN}{dt \, d\epsilon \, dV} = m_e c^2 \epsilon^2 f_{esc}(\epsilon) \int_{m_{min}}^{m_{max}} dm \; \xi(m) \times \int_z^{z_{max}} dz_1 \left| \frac{dt_*}{dz_1} \right| \psi(z_1) \; \dot{N}_\star(\epsilon; m, t_\star(z, z_1)) \; . \quad (4)$$

The luminosity density is dependent on the initial mass function (IMF), $\xi(m)$, the comoving star formation rate (SFR) density (i.e., the star formation rate per unit comoving volume), $\psi(z)$, and the fraction of photons which escape a galaxy, $f_{esc}(\epsilon)$ and avoid being absorbed by interstellar dust. The relationship between cosmic time and redshift is given by

$$\left| \frac{dt_*}{dz} \right| = \frac{1}{H_0 (1+z) \sqrt{\Omega_m (1+z)^3 + \Omega_\Lambda}} \; , \qquad (5)$$

in a flat ΛCDM cosmology. We assume cosmological parameters $H_0 = 70$ km s^{-1} Mpc^{-3}, $\Omega_m = 0.3$, and $\Omega_\Lambda = 0.7$.

Driver et al. (2008) have applied the dust model of Popescu & Tuffs (2009) to a survey of $\sim 10^5$ nearby galaxies from the Millennium Galaxy Catalog (Allen et al. 2006) to determine the wavelength-dependent escape fraction of photons in the local universe. RDF09 have fit this with a series of power-laws and we use this to compute $f_{esc}(\epsilon)$. We also assume that any photon with $m_e c^2 \epsilon > 13.6$ eV is absorbed by galactic and intergalactic H I gas. These UV photons are not re-

processed in our model, and we assume their net energy makes a small contribution to the total EBL intensity.

In this work we choose the limits of integration $m_{min} = 0.1$, $m_{max} = 100$, and $z_{max} = 6$, although our EBL intensities and luminosity density results at low z are not strongly dependent on the upper limits. Thus, the model of the stellar component does not have any adjustable parameters once an IMF and SFR have been chosen.

To test the accuracy of approximating stars as blackbodies and the simple Eggleton et al. (1989) stellar formulae, we computed the spectra of simple stellar populations (SSPs) for various ages from

$$L_\lambda(t_\star) = m_e c^2 \epsilon \frac{dN}{dt\, d\lambda} = \frac{m_e^2 c^4 \epsilon^3}{hc} \int_{m_{min}}^{m_{max}} dm\ \xi(m)\ \dot{N}_\star(\epsilon; m, t_\star) \qquad (6)$$

using a Salpeter (1955) IMF, i.e., $\xi(m) \propto m^{-2.35}$, from $m_{min} = 0.1 < m < m_{max} = 100$. Eqn. (6) approximates the spectrum of a cluster of stars that were all born at exactly the same time, and all now have an age of $t_\star$. SSPs at high spectral resolution were calculated by Bruzual & Charlot (2003) using various stellar spectral libraries calculated with detailed stellar structure codes. The Bruzual & Charlot (2003) SSPs with solar metalicity are compared with our approximations in Fig. 1. Our approximations agree fairly well longward of $\sim 10^3$ Å (0.1 μm), particularly for stars between 1 and 10 Gyrs of age. This age range of stars when weighted by the SFR dominates the radiative output between 0.1 and 10 μm, and this is where our approximations are best. Shortward of this wavelength the agreement is poor, as large as several orders of magnitude. However, at $\lesssim 0.1$ μm most photons will be absorbed by H I gas at low z, and at high z where stellar populations are younger agreement is much better at these wavelengths, differing by no more than a factor of ∼2–3. We have computed a test EBL model using a Salpeter IMF for both the blackbody approximation and using the Bruzual & Charlot (2003) SSPs and found that the difference is no more than $\approx 25\%$. As we show below, this is larger than the difference without including post-main sequence stars (§ 3.3). We therefore consider our blackbody approximation quite good for calculating luminosity densities and EBL energy densities, particularly compared to other uncertainties in these calculations.

2.2. *Dust Emission*

The starlight that is absorbed by dust is reradiated in the infrared. There are generally thought to be three major dust components in the interstellar medium (e.g. Desert et al. 1990): (1) a large grain component that absorbs optical light and reradiates in the far-IR, found in and around star-forming regions; (2) A small grain component that absorbs the far UV and reradiates in the near-IR, located throughout the disk of spiral galaxies and is responsible for most of the observed dust radiation and (3) a component from polycyclic aromatic hydrocarbons (PAHs) which emit as broad emission lines and are not generally in thermodynamic equilibrium with their environment (Dwek et al. 1997), although they are sometimes modeled as very hot blackbodies (e.g. Kneiske et al. 2002).

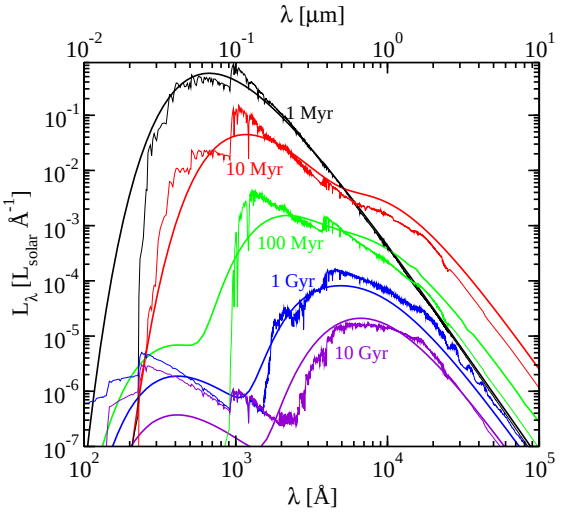

FIG. 1.— SSP spectra for various population ages, for a Salpeter IMF, normalized to 1 $M_\odot$. The thin lines are the models from Bruzual & Charlot (2003) and the thick lines are our calculations assuming stars are blackbodies. Photons with wavelengths shortward of 912 Å (13.6 eV) contribute a negligible amount to the total energy budget and are assumed to be completely absorbed.

We assume the dust emits as a combination of three blackbodies, representing three types of dust: a 40 K blackbody representing warm, large dust grains, a 70 K blackbody representing hot, small dust grains, and a 450 K blackbody representing PAHs. These temperatures are similar to those used by Kneiske et al. (2002). By setting the luminosity density from dust emission equal to the luminosity density from starlight absorbed from dust, we calculate the infrared emission self-consistently. The emissivity absorbed by dust is

$$\int d\epsilon\, \frac{1}{f_{esc}(\epsilon)} \left[1 - f_{esc}(\epsilon)\right]\, j^{stars}(\epsilon; z)$$

where $j^{stars}(\epsilon; z)$ is the stellar emissivity (§ 2.1). A fraction of this will be reradiated in each component, so that

$$f_n \int d\epsilon\, \frac{1}{f_{esc}(\epsilon)} [1 - f_{esc}(\epsilon)]\, j^{stars}(\epsilon; z) = \int d\epsilon\, j_n(\epsilon; \Theta_n) \qquad (7)$$

where f_n is the fraction of the absorbed emissivity reradiated in a particular dust component, $\Theta_n = k_B T_n / m_e c^2$ is the dimensionless temperature of the dust component, and the subscripts n =1, 2, and 3 refer to the warm dust, hot dust, and PAHs, respectively. Since the dust radiates as a blackbody, i.e.,

$$j_n(\epsilon; \Theta_n) = j_n^0 \frac{\epsilon^3}{\exp[\epsilon/\Theta_n] - 1}\ , \qquad (8)$$

the integral in the right side of eqn. (7) can readily be performed, so that

$$\int_0^\infty d\epsilon\, j_n(\epsilon; \Theta_n) = \frac{\pi^4}{15} j_n^0 \Theta_n^4\ . \qquad (9)$$

This allows one to determine the blackbody normaliza-

tion,

$$j_n^0 = 15 \frac{f_n \int d\epsilon \, \left[\frac{1}{f_{esc}(\epsilon)} - 1\right] \, j^{stars}(\epsilon; z)}{\pi^4 \Theta_n^4} \, . \quad (10)$$

Hence, the comoving luminosity density due to dust is

$$\epsilon \, j^{dust}(\epsilon; z) = \frac{15}{\pi^4} \int d\epsilon \, \left[\frac{1}{f_{esc}(\epsilon)} - 1\right] \times j^{stars}(\epsilon; z) \sum_{n=1}^{3} \frac{f_n}{\Theta_n^4} \, \frac{\epsilon^4}{\exp[\epsilon/\Theta_n] - 1} \, . \quad (11)$$

We assume that f_{esc}, f_n, and Θ_n do not vary with z. The values for f_n and Θ_n were chosen by trial and error to fit the IR luminosity density data at $z = 0.0$ and $z = 0.1$ (see § 3.1). These values can be found in Table 1. With the stellar component of the luminosity density calculated from eqn. (4), the dust component of the luminosity density can be determined. Both the stellar and dust luminosity densities are used to model the EBL energy density.

2.3. *Extragalactic Background Light Model*

The comoving EBL energy density at the current epoch can be obtained by integrating the luminosity density, eqns. (4) and (11),

$$\epsilon \, u_{EBL}(\epsilon; z = 0) = m_e c^2 \epsilon^2 \, \frac{dN}{d\epsilon \, dV} = \int_0^{z_{max}} dz_1 \, \frac{\epsilon' \, j(\epsilon'; z_1)}{(1 + z_1)} \, \left|\frac{dt_*}{dz_1}\right| \quad (12)$$

where $\epsilon \, j(\epsilon; z) = \epsilon \, j^{stars}(\epsilon; z) + \epsilon \, j^{dust}(\epsilon; z)$ and $\epsilon' = (1 + z_1)\epsilon$. If star formation and star emission ended at some redshift $z > 0$, then the EBL energy density observed today would be

$$\epsilon \, u_{EBL}(\epsilon; z) = \int_z^{z_{max}} dz_1 \, \frac{\epsilon' j(\epsilon'; z_1)}{(1 + z_1)} \, \left|\frac{dt_*}{dz_1}\right| \, . \quad (13)$$

This is the energy in the comoving frame per unit comoving volume as a function of ϵ, which is the photon energy in the comoving frame. The energy and volume in the comoving frame are quantities in coordinates which expand with the universe, and hence are the quantities which we observe today.

However, observers in a galaxy at a redshift $z > 0$ would have viewed a universe that is $(1+z)^3$ smaller than now, and photons observed now with energy ϵ would be observed by them to have proper energy $\epsilon_p = (1 + z)\epsilon$. The proper energy density they would have observed is given by

$$\epsilon_p \, u_{EBL,p}(\epsilon_p; z) = (1 + z)^4 \, \epsilon \, u_{EBL}(\epsilon; z) = (1 + z)^4 \int_z^{z_{max}} dz_1 \, \frac{\epsilon' j(\epsilon'; z_1)}{(1 + z_1)} \, \left|\frac{dt_*}{dz_1}\right| \quad (14)$$

where

$$\epsilon' = \epsilon(1 + z_1) = \frac{1 + z_1}{1 + z} \epsilon_p \, .$$

This is the radiation field with which a γ-ray photon emitted at redshift z interacts on its way to Earth.

TABLE 1
Dust Parameters. See text for details.

Component	n	f_n	T_n [K]	Θ_n [10^{-9}]
Warm Large Grains	1	0.60	40	7
Hot Small Grains	2	0.05	70	12
PAHs	3	0.35	450	76

Energy density can be converted to intensity in units of, e.g., nW m^{-2} sr^{-1} by

$$\epsilon \, I(\epsilon; z) = \frac{c}{4\pi} \, \epsilon \, u_{EBL}(\epsilon; z) \, , \quad (15)$$

which is convenient for comparing to EBL intensity measurements.

3. NUMERICAL RESULTS

In this section, we compute the luminosity densities and EBL energy densities from starlight and dust for various combinations of SFRs and IMFs. Although the Salpeter (1955) IMF ($\xi(m) \propto m^{-2.35}$) is still in common use, it now seems that it overpredicts the number of low mass stars. Baldry & Glazebrook (2003) fit local luminosity density data to find a preferred IMF, which is similar to a Salpeter IMF above $m = 0.5$ ($\xi(m) \propto m^{-2.2}$) but flatter below this mass ($\xi(m) \propto m^{-1.5}$). The Salpeter A IMF is also often used, which is $\xi(m) \propto m^{-0.5}$ below $m = 0.5$ and $\xi(m) \propto m^{-2.35}$ above $m = 0.5$. Hopkins & Beacom (2006) compiled a large amount of SFR data and fit them using various IMFs. To parameterize their SFR fits they used the function of Cole et al. (2001) as well as their own piecewise power-law function, and found the Salpeter A and Baldry & Glazebrook (2003) IMFs were favored, under the assumption of a universal IMF.

For our models we use the same designations as RDF09 which are as follows (see RDF09 for details on these SFRs and IMFs):

- *Model A*: Cole et al. (2001) SFR and Salpeter A IMF
- *Model B*: Hopkins & Beacom (2006) SFR using Cole et al. (2001) parameterization and Salpeter A IMF
- *Model C*: Hopkins & Beacom (2006) SFR using Cole et al. (2001) parameterization and Baldry & Glazebrook (2003) IMF.
- *Model D*: Hopkins & Beacom (2006) SFR and Salpeter A IMF
- *Model E*: Hopkins & Beacom (2006) SFR and Baldry & Glazebrook (2003) IMF

Measurements of SFRs are generally only sensitive to the formation of massive stars, so that an IMF must be chosen to extrapolate to lower masses and determine the global SFR. Thus, the SFR and IMF are not independent of one another and a combination of both are needed to calculate luminosity densities and EBL energy densities.

3.1. *Luminosity Density*

The luminosity density at a particular wavelength is measured by adding up the luminosities of the galaxies at that wavelength in a particular volume, and forming a luminosity function using the $1/V_{max}$ method (e.g., Sandage et al. 1979). This involves finding the luminosities within a redshift slice, which gives the maximum comoving volume (V_{max}) within which the galaxies could be found. Since the surveys are limited to a minimum observable magnitude, some extrapolation to lower luminosities must be done, which involves a fit to the luminosity function. In the optical and UV, the luminosity function is typically fit with a Schechter (1976) function which is

$$\phi(L) = \frac{\phi_* \ (L/L_*)^\alpha \ \exp(-L/L_*)}{L_*} \ , \tag{16}$$

where the function has three fit parameters, ϕ_*, L_*, and α. This function can be integrated to give the luminosity density, so that

$$j_\epsilon = \int_0^\infty \ dL \ L \ \phi(L) = \phi_* L_* \Gamma(\alpha + 2) \tag{17}$$

where $\Gamma(x)$ is the Gamma function. The Schechter function, written in terms of absolute magnitude, M (not to be confused with stellar mass in § 2), is

$$\begin{aligned} \phi(M) = 0.4 \ln(10) \phi_* 10^{0.4(M-M_*)(\alpha+1)} \\ \times \exp(-10^{-0.4(M-M_*)}) \ , \end{aligned} \tag{18}$$

which can then be integrated to give the luminosity density in terms of AB magnitudes per volume,

$$j_M = M_* - 2.5 \log \left[\phi_* \Gamma(\alpha + 2)\right] + C \tag{19}$$

where C is the conversion from observed magnitudes to AB magnitudes. The error in the luminosity density is

$$\begin{aligned} \sigma^2_{j_M} &= \left(\frac{\partial j}{\partial M_*}\sigma_{M_*}\right)^2 + \left(\frac{\partial j}{\partial \phi_*}\sigma_{\phi_*}\right)^2 + \left(\frac{\partial j}{\partial \alpha}\sigma_\alpha\right)^2 \\ &= \sigma^2_{M_*} + \left(\frac{2.5}{\ln(10)}\frac{\Gamma(\alpha+2) \ \sigma_{\phi_*}}{\phi_*}\right)^2 + \\ &\quad \left(\frac{2.5}{\ln(10)}\psi_0(\alpha+2) \ \sigma_\alpha\right)^2 \ , \end{aligned} \tag{20}$$

where $\psi_0(x)$ is the digamma function (not to be confused with $\psi(z)$, the SFR, used in § 2.1). This can be converted to power per volume (in, e.g., W Mpc^{-3}) by

$$\epsilon j_\epsilon = \nu \ \times \ 10^{\frac{j_M - 34.10}{-2.5}} \tag{21}$$

and

$$\sigma_{\epsilon j_\epsilon} = \frac{\nu \ln(10)}{-2.5} \ 10^{\frac{j_M - 34.10}{-2.5}} \ \sigma_{j_M} \tag{22}$$

where ν is the central frequency of the bandpass.

Luminosity functions in the IR can be quite different from the optical, and are often fit with broken power-laws,

$$\phi(L) = \begin{cases} \phi_* \ \left(\frac{L}{L_*}\right)^{1-\alpha} & L < L_* \\ \phi_* \ \left(\frac{L}{L_*}\right)^{1-\beta} & L > L_* \end{cases} \ , \tag{23}$$

(e.g., Babbedge et al. 2006) instead of a Schechter function. Integrating this, then, to get the luminosity density gives

$$\epsilon \, j_\epsilon = \int dL \ \phi(L) = \phi_* L_* \left\{ \frac{1}{2-\alpha} - \frac{1}{2-\beta} \right\} \ , \tag{24}$$

assuming $\beta > 2$. Aside from direct observations, the UV luminosity density at high redshift can be probed with measurements of the photoionization rate from the Lyα forest (Faucher-Giguère et al. 2008a,b).

In terms of our theoretical formalism, the luminosity density is dependent on the IMF, SFR, and dust parameters, and can be calculated from eqns. (4) and (11). The results of our models, plotted with measurements of the luminosity density at various redshifts, can be seen in Figs. 2 and 3. Although the differing measurements do not entirely agree, they provide a consistent picture for the evolution of the luminosity density, particularly in the UV/optical and at low redshift.

It appears that our Model C best fits the luminosity density data. Models C and E fit the data about equally well at most wavelengths, but model C fits the UV data at low redshift (especially $z = 0.1$) better than does model E. These models agree with the data quite well at low z, and less-well at high z; however, Model C still provides a better fit to the data at high z than do the other models. Measurements at higher redshifts are less certain, and less likely to agree with each other. Interestingly, the luminosity densities at high z from Lyα measurements (Faucher-Giguère et al. 2008b) are about a factor of two higher than measurements from direct imaging. Faucher-Giguère et al. (2008b) speculate that this may be due to a faint population of galaxies at high redshift which have avoided detection in deep surveys so far. Other possible explanations for a discrepancy at high z include a changing IMF, and a changing absorption from dust; we assume both of these are independent of redshift in our models. The 24 μm luminosity density from Babbedge et al. (2006) increases rapidly at high z, and is considerably above our models and other data.

The higher redshift luminosity density contributes little to the local EBL. Thus such discrepancies have little effect on the direct EBL observations (§ 3.2) and absorption of TeV γ-rays from nearby blazars (§ 4), although it could have implications for absorption of γ-rays from higher z objects observed with *Fermi* or *AGILE*, however, even here generally only for the UV/optical.

3.2. *Extragalactic Background Light*

Direct measurement of the EBL energy density is difficult due to contamination from foreground zodiacal and Galactic light (Bernstein et al. 2002; Gorjian et al. 2000; Dwek & Arendt 1998; Cambrésy et al. 2001; Wright & Reese 2000; Levenson et al. 2007; Hauser et al. 1998). For example, the foreground subtraction of the optical measurements of the EBL with the *Hubble Space Telescope* by Bernstein et al. (2002) have been vigorously debated (Mattila 2003; Bernstein et al. 2005; Bernstein 2007). The most accurate IR-to-UV EBL measurements are the measurements of the far-IR with COBE (Fixsen et al. 1998) and BLAST (Marsden et al. 2009). Galaxy counts may be used to estimate the EBL (Madau & Pozzetti 2000;

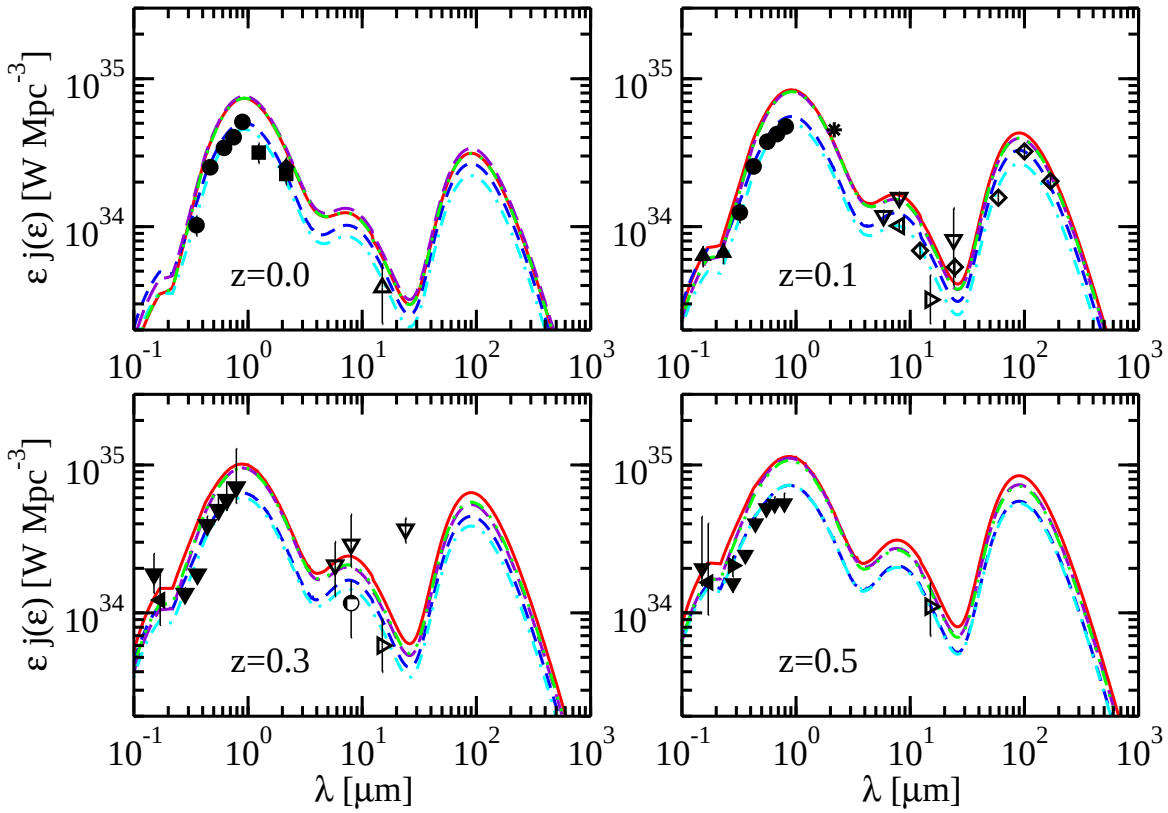

FIG. 2.— Data and models of the comoving luminosity density at various redshifts. Data are black symbols with error bars, as follows: filled circles: Blanton et al. (2003); filled squares: Cole et al. (2001); filled diamonds: Kochanek et al. (2001); filled upward-pointing triangles: Budavári et al. (2005); filled downward-pointing triangles: Tresse et al. (2007); filled leftward-pointing triangles: Sawicki & Thompson (2006); filled rightward-pointing triangles: Dahlen et al. (2007); star: Smith et al. (2008); empty upward-pointing triangles: Magnelli et al. (2009); empty diamonds: Takeuchi et al. (2006); empty downward-pointing triangles: Babbedge et al. (2006); empty leftward-pointing triangles: Huang et al. (2007); empty rightward-pointing triangles: Le Floc'h et al. (2005); circle with cross inside: Flores et al. (1999). Curves are our models as follows: solid red: Model A; Dashed double-dotted green: Model B; short dashed blue: Model C; long dashed violet: Model D; dashed-dotted cyan: Model E.

Fazio et al. 2004; Dole et al. 2006; Metcalfe et al. 2003; Papovich et al. 2004) but the crowded fields make this difficult, and the unknown number of unresolved sources results in a lower limit. Levenson & Wright (2008) have used a Monte Carlo Markov chain analysis to correct for crowded fields in 3.6 μm galaxy counts with the *Spitzer Space Telescope*, resulting in significantly stronger lower limits. Their new technique, when applied to other wavelengths, could drastically improve estimates of the EBL. Still, the lower limits from galaxy counts, even the improved one by Levenson & Wright (2008), are a factor of a few below the direct measurements. This indicates either that a significant fraction of the EBL originates from extremely faint galaxies not resolved in number counts, or there is significantly more foreground light than assumed. Franceschini et al. (2008) consider the latter to be more likely, based on the fact that the galaxy counts are performed in fields with quite deep exposures.

The EBL photon density, calculated with our models, can be seen in Fig. 4, along with direct measurements, lower limits from galaxy counts, and upper limits from TeV blazar observations. Models C and E are very close to the galaxy count lower limits in the optical and UV, and in fact are below the near-IR lower limits from Levenson & Wright (2008) and the far-IR limits from Dole et al. (2006). Models A, B, and D, on the other hand, seem to be marginally above the upper limits from γ-ray observations of blazars (Mazin & Raue 2007; Finke & Razzaque 2009) although these results are not without controversy (e.g., Stecker & Scully 2008). Due to how well Model C fit the luminosity density data, we take this as our best fit model.

The integrated intensity from our models can be seen in Table 2. Fardal et al. (2007) created a simple model by a fit which compromises between direct photometric observations and number-count lower limits on the local EBL intensity. They find an integrated EBL intensity of 50 – 130 nW m^{-2} sr^{-1}, and a value closer to the lower end is required to be consistent with the K-band luminosity density (similar to our best fit model, model C). Nagamine et al. (2006) find this value to be 43 $\pm$ 7 nW m^{-2} sr^{-1}, which is in good agreement with our model C.

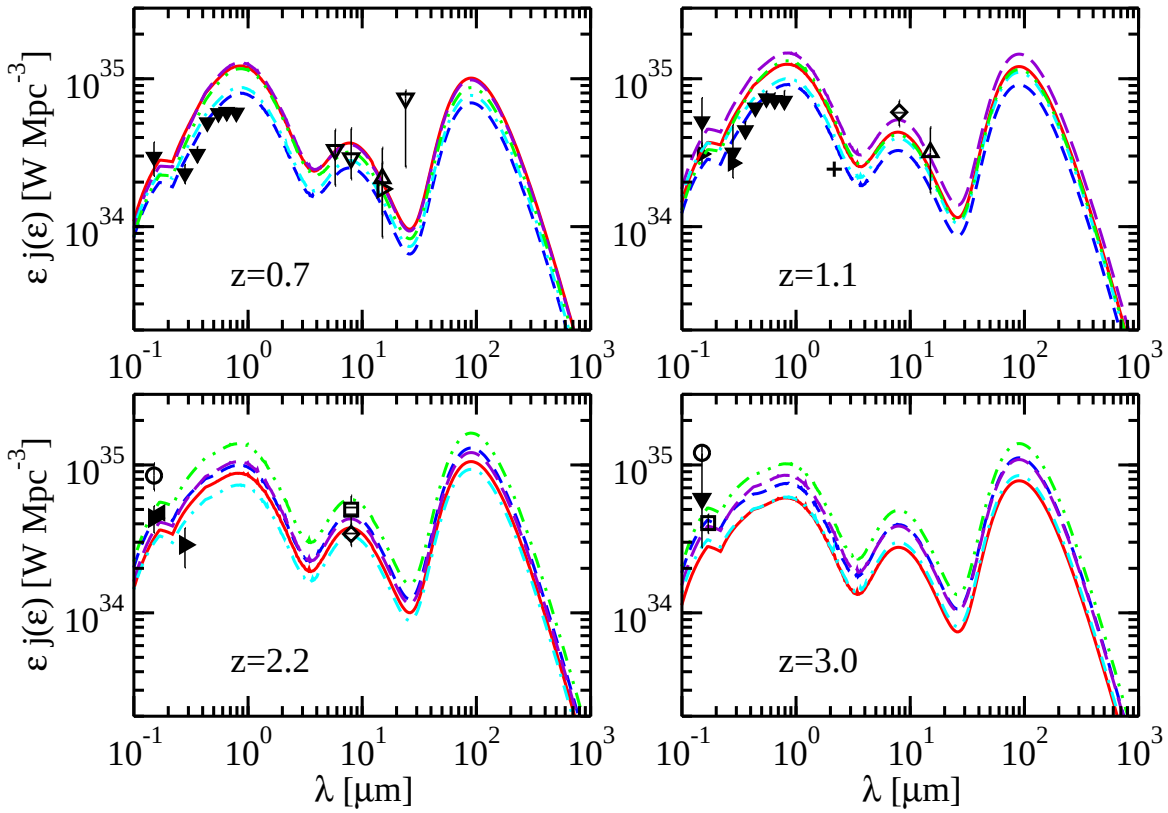

FIG. 3.— Data and models of the comoving luminosity density at various redshifts. Symbols and curves are the same as Fig. 2, while additional data are from the following sources: cross: Cirasuolo et al. (2007); empty circles: Faucher-Giguère et al. (2008a,b); empty square: Reddy et al. (2008); diamonds with horizontal stripes: Caputi et al. (2007). box with horizontal stripes: Pérez-González et al. (2005).

Our model of the stellar component is more accurate at low redshifts than high redshifts, and more accurate than the dust component, since there are more luminosity density data in this region with which to normalize our results. Results from our best fit model are in quite good agreement with lower limits from galaxy counts in the near-IR through UV, except for the recent 3.6 μm point of Levenson & Wright (2008). In the far IR, this model is slightly below the points of Dole et al. (2006), although they do fit the BLAST data (Marsden et al. 2009) fairly well. The addition of a separate component representing ultraluminous infrared galaxies, as done by Kneiske et al. (2004), may bring our model C in agreement with these other lower limits. However, it is unclear why this component would not be represented in the luminosity density measurements (Figs. 2 and 3). Krennrich et al. (2008) have recently used the lower limit of Levenson & Wright (2008) to construct their own EBL SED, which gives a greater energy density than our model C.

Fig. 5 shows the redshift evolution of model C. This peaks at around $z \approx 2$, which is about where the SFR peaks (see RDF09). Also note that at higher redshifts, there are more high mass stars to create a larger high energy component. The high z SEDs are flatter in the optical-UV due to this relatively higher contribution of high mass stars. At lower z, the contribution is greater from longer living low mass stars, as well as those high mass stars which have evolved off the main sequence. This also affects the dust emission component. At around $z = 1$ the far-IR dust component peaks at a greater energy density than does the optical stellar component, and the mid-IR PAH component gets progressively greater at higher z. Since the dust absorption is greater at higher energy (lower wavelength), where the high mass stars emit most of their radiation, the absorption is greater at higher z, and thus the dust emission is greater at higher z.

The Balloon-borne infrared telescope BLAST found that the fraction of galaxies with redshift $z < 1.2$ which contribute to the local EBL is $f_{EBL}(z < 1.2, 250\ \mu m) = 0.60 \pm 0.11$, $f_{EBL}(z < 1.2, 350\ \mu m) = 0.49 \pm 0.10$, and $f_{EBL}(z < 1.2, 500\ \mu m) = 0.39 \pm 0.11$, where the error bars include measurement and calibration uncertainties (Marsden et al. 2009). We calculate these fractions for our model C, to test its consistency with these BLAST results, with

$$f_{EBL}(< z, \epsilon) \equiv \frac{\int_0^z dz_1 \ \frac{\epsilon' \, j(\epsilon'; z_1)}{(1+z_1)} \ \left| \frac{dt_*}{dz_1} \right|}{\epsilon \, u_{EBL}(\epsilon; z = 0)} \qquad (25)$$

Results from this calculation can be seen in Fig. 6. As

TABLE 2
Integrated EBL intensity from our models, in nW m^{-2} sr^{-1}.

Model	Stellar Component	Dust Component	Total
A	36.0	25.9	61.9
B	36.4	25.5	61.8
C	26.5	20.4	46.8
D	37.0	26.1	63.1
E	25.5	19.6	45.0

can be seen, these fractions are in excellent agreement with the results from BLAST.

3.3. *Comparison with other models*

We have plotted our best fit model, Model C, along with several other models from the literature in Fig. 7. Note that our model agrees remarkably well with those of Franceschini et al. (2008) and Gilmore et al. (2009) at $\gtrsim 0.3$ eV ($\lesssim 5$ μm). Of the models presented in Fig. 7, only the best fit model of Kneiske et al. (2004) and the fast evolution model of Stecker et al. (2006) agree with the recent 3.6 μm lower limit from Levenson & Wright (2008).

Two previous models from RDF09 are plotted here, using the single power-law version of the stellar luminosity-mass relation. These previous versions of our model include the contribution to the EBL from main-sequence stars. Model B from RDF09 was considered our best fit model from this previous work, while we have plotted the old Model C for comparison with our best fit model from this work. It is clear that post-main sequence stars have a considerable effect on the result, as the C models differ by as much as an order of magntitude at longer wavelengths ($\sim 1 - 10$ μm). The model in this work is more intense longward of ~ 1 μm due mainly to giant stars, while shortward of ~ 0.3 μm the inclusion of white dwarfs explains the discrepancy between these works.

The modeling technique of Kneiske et al. (2002, 2004) is quite similar to ours: they also integrate over stellar parameters and treat dust extinction and re-emission in a similar fashion. Our results, however, differ significantly from theirs due to our use of updated parameters for the SFR, IMF and dust extinction. The best fit model of Kneiske et al. (2004) also includes separate components from ultraluminous infrared galaxies (ULIGs) and normal galaxies, which, if applied to our model (as mentioned above), could result in a local EBL energy densities more in agreement with the lower limits of Dole et al. (2006) and Levenson & Wright (2008), with which the Kneiske et al. (2004) best fit model is in agreement. Their infrared component, however, considerable overpredicts the 250 μm measurements from BLAST (Marsden et al. 2009) and COBE (Fixsen et al. 1998). Disentangling the dust extinction from these two different populations, using the realistic Driver et al. (2008) (or the Popescu & Tuffs 2009) model would be considerably more complicated. Furthermore, greater dust emission may contradict the luminosity density data at low z (Fig. 2).

Stecker et al. (2006) have used a backwards evolution model based on observations of the infrared luminosity function to calculate the IR EBL energy density. They then use a forward evolution model similar to Salamon & Stecker (1998) to calculate the optical/UV EBL, and normalize it to their backward-evolution calculation. Our model peaks in the IR at an intensity relatively close to their baseline model, both of which are below the IR lower limits of Dole et al. (2006). However, our models differ by as much as a factor of 8 in the UV. This could be because extrapolating below 10 μm may not be appropriate for determining the infrared background (Lagache et al. 2003). This wavelength is critically important to the models of Stecker et al. (2006) because this is where they normalize the results of their forward-evolution modeling, and the optical/UV region is the most important for γ-ray absorption (§ 4). Furthermore, their model has neglected dust extinction, which has a considerable effect at UV wavelengths. We note that the far IR peak of their baseline model, which is based in IR luminosity density data, is within 10% of our far-IR peak, which is fit to similar IR luminosity density data.

Gilmore et al. (2009) have presented models based on semi-analytic models of galaxy evolution, using cosmological parameters from WMAP and normalizing their semi-analytic model's luminosity density prediction to local luminosity density measurements. They also include a component from quasars and realistically treat extinction of ionizing radiation by the intergalactic medium, both of which have implications for the UV portion of the EBL at high redshift. Gilmore et al. (2009) only treat the UV-optical portion of the EBL, while their further work will be presented in Gilmore et al. (in preparation). This is an update of previous, similar models (Primack et al. 1999, 2001, 2005). The stellar component of our model probably agrees with the Gilmore et al. (2009) fiducial model so well because we have both made sure our models agree well with luminosity density measurements (§ 3.1). However, at lower energies (longer wavelengths) their model intensity is as much as double ours. Moreover, their predicted intensity is above the 250 μm BLAST measurement (Marsden et al. 2009), although it is consistent with the COBE results (Fixsen et al. 1998).

The model of Franceschini et al. (2008) is based on integrating luminosity functions at various wavelengths and redshifts to generate an EBL energy density. Again, their model agrees well with ours at higher energies but at 20 μm they predict about three times the intensity as we do. The infrared component of their model is comparable to that of the best fit model of Kneiske et al. (2004), and similarly, it over-predicts the 250 μm BLAST (Marsden et al. 2009) measurement and the COBE (Fixsen et al. 1998) infrared data.

4. ABSORPTION OF γ-RAYS

Once the energy density of the EBL has been calculated using eqn. (14), the absorption optical depth of γ-ray photons as a function of observed γ-ray photon energy, ϵ_1, can be calculated by

$$\tau_{\gamma\gamma}(\epsilon_1, z) = \frac{c\pi r_e^2}{\epsilon_1^2 m_e c^2} \int_0^z \frac{dz'}{(1+z')^2} \left|\frac{dt_*}{dz'}\right| \times \int_{\frac{1}{\epsilon_1(1+z')}}^{\infty} d\epsilon_p \frac{\epsilon_p u_{EBL,p}(\epsilon_p; z')}{\epsilon_p^4} \bar{\phi}(\epsilon_p \epsilon_1 (1+z')) \ , \quad (26)$$

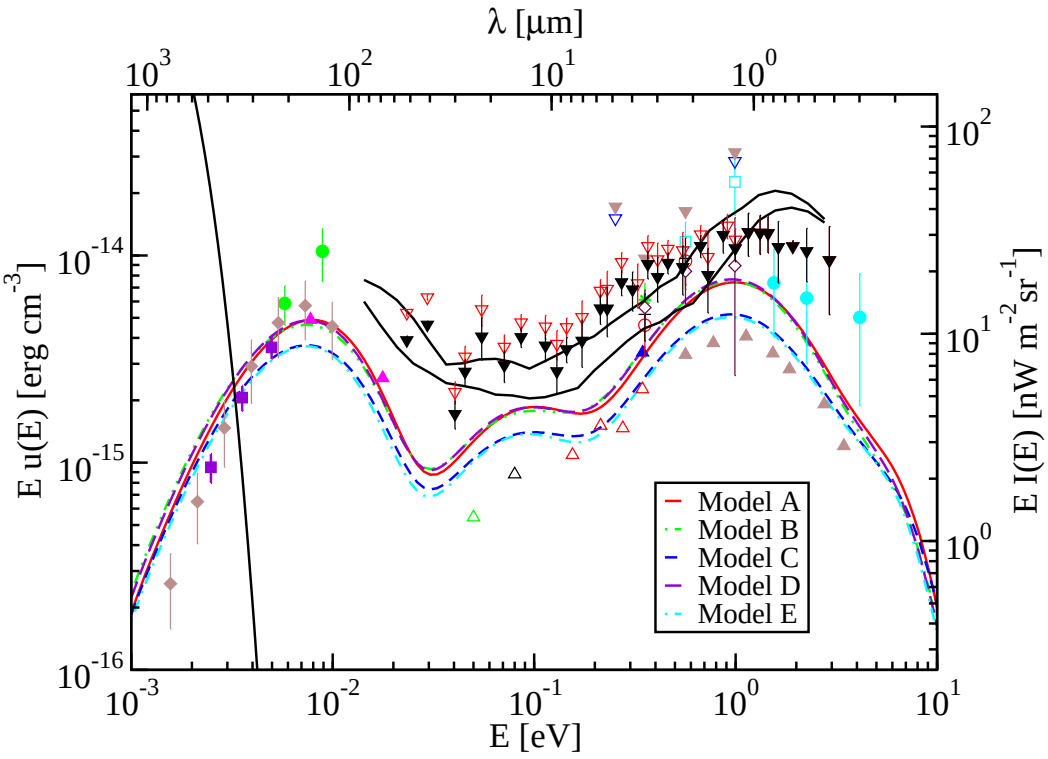

FIG. 4.— Our models for the EBL plotted along with measurements and constraints from observations. The curves are our models with the same symbols as Fig. 2. Measurements are from Bernstein et al. (2002, cyan points), Gorjian et al. (2000, empty red circle), Dwek & Arendt (1998, green asterisk), Cambrésy et al. (2001, empty cyan square), Wright & Reese (2000, black cross), Levenson et al. (2007, maroon diamonds), Hauser et al. (1998, green filled circles), Fixsen et al. (1998, brown filled diamonds), and Marsden et al. (2009, violet filled squares). Lower limits are from Fazio et al. (2004, red empty triangles), Madau & Pozzetti (2000, brown filled triangles), Levenson & Wright (2008, blue filled triangle), Dole et al. (2006, magenta filled triangles), Metcalfe et al. (2003, black empty triangle), and Papovich et al. (2004, green empty triangle). Upper limits are from Hauser et al. (1998, brown filled inverted triangles), Dwek & Arendt (1998, blue empty inverted triangles), Mazin & Raue (2007, upper and lower black curves $\Gamma_{int}^{min} = 0.67$ and $\Gamma_{int}^{min} = 1.5$ upper limits, respectively), and red empty and black filled inverted triangles are the $\Gamma_{int}^{min} = 1.0$ and $\Gamma_{int}^{min} = 1.5$ upper limits, respectively, from Finke & Razzaque (2009). The black curve at long wavelengths is the cosmic microwave background.

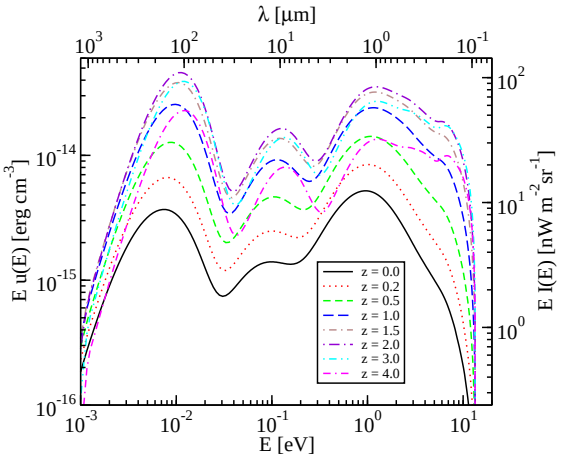

FIG. 5.— The proper EBL energy density as a function of proper photon energy for model C, for a variety of redshifts.

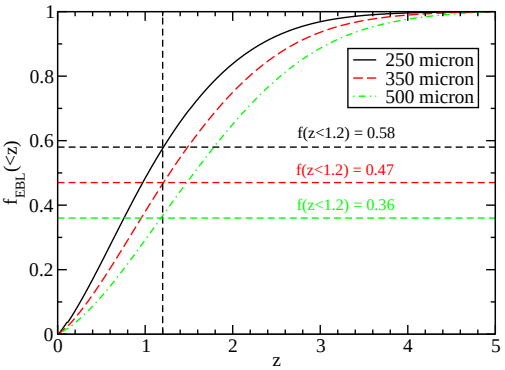

FIG. 6.— The fraction of the local ($z = 0$) EBL which originates below a redshift z at the three BLAST wavebands (Marsden et al. 2009) for our model C.

where $|dt_*/dz|$ is given by eqn. (5), ϵ^p is the proper frame EBL photon energy, $\epsilon^p\, u^p_{EBL}(\epsilon^p; z')$ is the proper frame EBL energy density given by eqn. (14),

$$\bar{\phi}(s_0) = \frac{1+\beta_0^2}{1-\beta_0^2} \ln w_0 - \beta_0^2 \ln w_0 - \frac{4\beta_0}{1-\beta_0^2} \qquad (27)$$
$$+2\beta_0 + 4 \ln w_0 \ln(1+w_0) - 4L(w_0) \ ,$$

$\beta_0^2 = 1 - 1/s_0$, $w_0 = (1+\beta_0)/(1-\beta_0)$, and

$$L(w_0) = \int_1^{w_0} dw\ w^{-1} \ln(1+w) \qquad (28)$$

(Gould & Schréder 1967; Brown et al. 1973).

We have used our model C to deabsorb several of the blazars presented in Finke & Razzaque (2009). We choose blazars that have a low ξ parameter, defined in

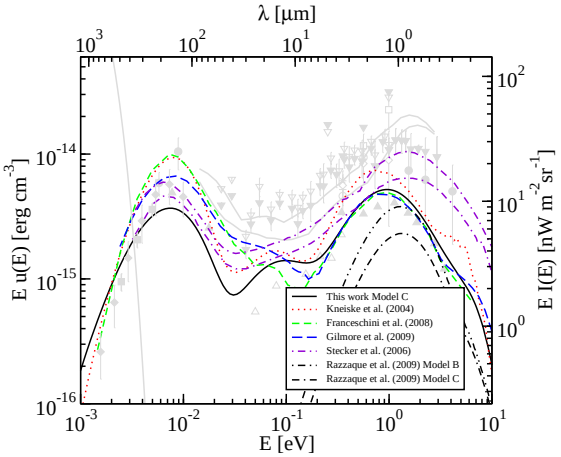

FIG. 7.— Our model C (solid black curve), the best fit model of Kneiske et al. (2004, red dotted curve), the model of Franceschini et al. (2008, short dashed green curve), the fiducial model of Gilmore et al. (2009, long dashed blue curve) and the fast evolution and baseline model from Stecker et al. (2006, upper and lower dot-dashed violet curves, respectively). The double dot-dashed and the dot double-dashed black curves are the single power-law model B and model C from RDF09, respectively.

Finke & Razzaque (2009) to be

$$\xi = \left(\frac{TeV}{E_{max}}\right) \frac{\Gamma_{obs} - \Gamma_{int}^{min}}{z} \ln\left(\frac{E_{max}}{E_{min}}\right) \ , \qquad (29)$$

(not to be confused with $\xi(m)$, the IMF in § 2.1) where E_{min} and E_{max} are the minimum and maximum energies of the VHE γ-ray spectrum, Γ_{obs} is the observed photon spectral index, and Γ_{int}^{min} is an assumed minimum intrinsic photon spectral index, for which we use $\Gamma_{int} = 1.5$, the lowest value one would expect from naïve test particle shock acceleration theory where particles are accelerated with number indices steeper than -2 (for a review, see Blandford & Eichler 1987) although see Stecker et al. (2007) for a different interpretation. The lower the parameter ξ, the lower the deabsorbed spectral index Γ should be. We also choose the VHE γ-ray spectra of two bright, distant quasars, 3C 66A and 3C 279 to deabsorb, to give a greater range in redshift. The deabsorbed spectra are fit with power-laws, and the results can be seen in Fig. 8 and Table 3. Note that in Fig. 8 the νF_ν spectra is plotted, where $\Gamma = 1.5$ corresponds to $\nu F_\nu \propto E^{0.5}$. The results are generally consistent with a minimum intrinsic Γ_{int} of 1.5, as this value is within the error bars for all of the sources.

A plot of the energy at which the universe becomes optically thick to γ-rays, defined where $\tau_{\gamma\gamma} = 1$ is given in Fig. 9, which is often known as the Fazio-Stecker relation (Fazio & Stecker 1970), for several models including our Model C. Also plotted are the maximum photon energy bin of several blazars, observed with atmospheric Cherenkov telescopes (see Finke & Razzaque 2009, for a list and references) and the GRBs 080916C (Abdo et al. 2009b) and 090902B (Abdo et al. 2009a) observed with the *Fermi*-LAT. The VHE γ-rays from many blazars are highly attenuated by the EBL, since several are considerably above the $\tau_{\gamma\gamma} = 1$ for all models, and the highest energy photons from GRBs constrain the EBL at high redshifts. Also note that the universe will be optically thin to 20 GeV and lower photons over all redshifts for all models except those of Stecker et al. (2006).

We have plotted the absorption optical depth for our model and several others in Fig. 10. The models are optically thin ($\tau_{\gamma\gamma} < 1$) at 200 GeV for $z < 3$, except the models of Stecker et al. (2006). Observing a large number of high-energy photons with observatories such as *Fermi* and *AGILE* from high-z sources could rule out these models. Our model is moderately more opaque than those of Gilmore et al. (2009) and Franceschini et al. (2008) at these redshifts, although it would be difficult to distinguish these models based on γ-ray observations.

5. SUMMARY AND CONCLUSIONS

We have developed a model for the UV through far-IR EBL from direct stellar radiation and stellar radiation which is absorbed and reradiated by dust. This approach extends RDF09, which applied between $\sim$ 1–10 eV. Our best fit model, Model C, is consistent with the collection of measures of SFR by Hopkins & Beacom (2006), and a variety of luminosity density data at various redshifts $z \leq 3$. It does not require complex stellar structure codes or semi-analytic models of galaxy formation. Our model is most accurate at low-z and high ϵ (short wavelengths), which is the energy and redshift range that is useful for calculating the absorption of TeV γ-rays from nearby blazars by electron-positron pair production. The EBL energy density of Model C is generally consistent with lower-limits from galaxy counts and is below direct EBL measurements except for the lower limits at 3.6 μm (Levenson & Wright 2008) and 60 μm (Dole et al. 2006). It also agrees well with the recent EBL models of Gilmore et al. (2008) and Franceschini et al. (2008) in the near-IR through UV, although less well at longer wavelengths. Our Model C is significantly below the models of Kneiske et al. (2004) and Stecker et al. (2006) for all wavelengths.

The SFR, IMF, and dust parameters in our best fit EBL model were chosen to agree well with luminosity density measurements, particularly those at low-z where the data is best, and to give precedence to luminosity density measurements over local EBL measurements when deciding the quality of an EBL model. Although different luminosity density measurements are not always consistent with each other, as one can see in Figs. 2 and 3, they are less controversial than measurements of the local EBL intensity. For example, Madau & Pozzetti (2000) claim that their galaxy count measurements resolve almost all of the flux in the EBL. Bernstein et al. (2002) suggest, however, that those measurements fail to take into account the faint portions of the distant galaxies. The more direct measurements of Bernstein et al. (2002) give higher values than galaxy counts, but their measurements have also been criticized for the subtraction of zodiacal foreground light (e.g. Mattila 2003; Bernstein et al. 2005; Bernstein 2007). To reconcile these differing inferences, Totani et al. (2001) suggest the possibility that this discrepancy can be resolved by a faint EBL component outside of normal galaxy populations.

By constructing an EBL model consistent with luminosity-density observations, we have found that an EBL energy density very close to the lower limits from number counts is required. Similar conclusions were reached by Fardal et al. (2007). They point out that their results are strongly dependent on the

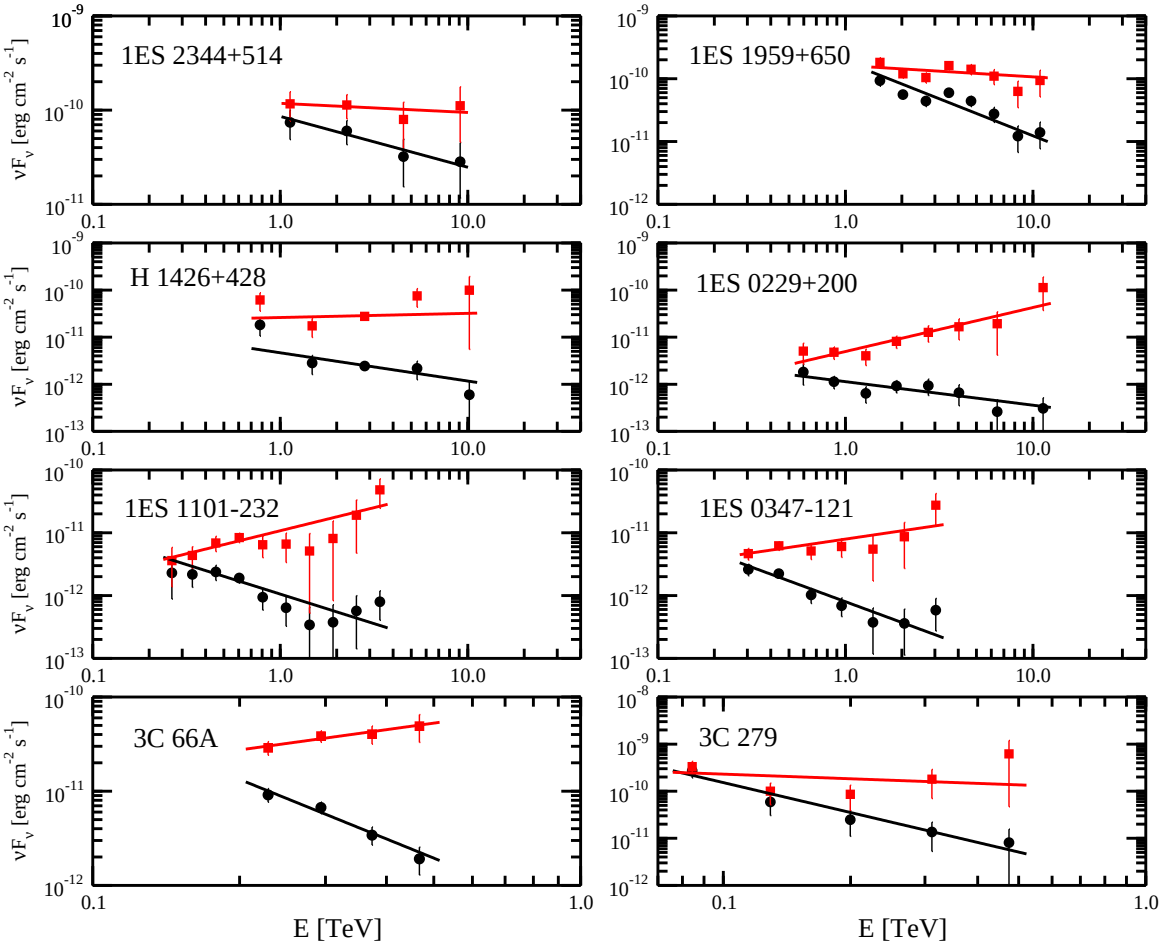

FIG. 8.— TeV blazar spectra observed (circles) and deabsorbed by our model C (squares).

TABLE 3
DEABSORBED TEV BLAZARS

Blazar	Redshift	Observed Γ	Deabsorbed Γ	ξ	Reference
1ES 2344+514	0.044	2.54 ± 0.18	2.10 ± 0.68	4.7	Schroedter et al. (2005)
1ES 1959+650	0.047	3.18 ± 0.17	2.18 ± 0.33	4.7	Aharonian et al. (2003a)
1ES 1426+428	0.129	2.60 ± 0.60	1.91 ± 0.58	2.2	Aharonian et al. (2003b)
1ES 0229+200	0.139	3.09 ± 0.26	1.07 ± 0.45	1.8	Aharonian et al. (2007c)
1ES 1101-232	0.186	2.94 ± 0.20	1.27 ± 0.46	5.7	Aharonian et al. (2007a)
1ES 0347-121	0.188	3.10 ± 0.25	1.56 ± 0.43	6.5	Aharonian et al. (2007b)
3C 66A	0.444[a]	4.10 ± 0.72	1.28 ± 0.98	19.6	Acciari et al. (2009)
3C 279	0.536	4.11 ± 0.68	2.33 ± 0.89	16.0	Albert et al. (2008)

IMF, which may vary over the history of the universe. Although radiation hydrodynamic simulations indicate that radiative feedback could lead to a universal IMF in the local universe (Bate 2009), a detailed modeling of a large amount of Sloan Digital Sky Survey data indicates that fainter galaxies generally have an IMF which produces fewer massive stars than brighter galaxies (Hoversten & Glazebrook 2008). This result has further evidence in the ratio of Hα to far-UV flux in H I-selected galaxies (Meurer et al. 2009). Babbedge et al. (2006) suggested that a non-universal IMF may be responsible for their measured rapid increase in the 24 μm luminosity density (§ 3.1).

Georganopoulos et al. (2008) have suggested a new method for measuring the EBL. They point out that Compton scattering of the infrared component of the EBL by the radio lobes of Fornax A could be detectable by *Fermi* in $\sim$ 2 years in scanning mode, and that it may also be possible to put upper limits on the optical EBL component in the absence of *Fermi* detection. This will be particularly important for distinguishing our best fit model from those which predict significantly higher IR emission, such as those of Kneiske et al. (2004) or Franceschini et al. (2008).

In the near future, surveys such as the Dark Energy Survey, and the Sloan Digital Sky Survey II will detect $\sim 10^3$ core-collapse supernovae per year, and Pan-STARRS and the Large Synoptic Survey Telescope

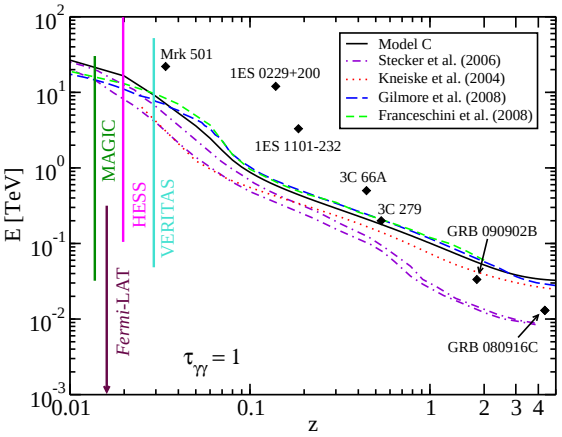

FIG. 9.— A plot of $\tau_{\gamma\gamma} = 1$ for several EBL models including our model C, as a function of redshift. Curves signify the same models as in Fig. 7. Also plotted by the filled diamonds are the maximum γ-ray photon energy bins from blazars observed with atmospheric Cherenkov telescopes and the GRBs 080916C and 090902B observed with the *Fermi*-LAT.

will detect $\sim 5 \times 10^5$ core-collapse supernovae per year (Lien & Fields 2009). This will lead to extremely precise measurement of the SFR, as the core collapse supernovae rate is a good tracer of the high mass SFR, although modeling dust attenuation will still be a significant challenge. This in turn will lead to strong constraints on models of the EBL and luminosity density. Detection of the neutrino background from core-collapse supernovae will further constrain the SFR and EBL (e.g., Horiuchi et al. 2008). Combinations of these various measurements mean that very soon the local EBL will be known to much greater precision.

We have used our best fit EBL model (Model C) to calculate the absorption optical depth to γ-rays from cosmological sources, valid over all relevant γ-ray energy ranges and redshifts. Our results show that absorption is quite significant for blazars observed at TeV energies by atmospheric Cherenkov telescopes, and that de-absorbed VHE blazar spectra give results generally in agreement with particle acceleration theory. We also find that the universe is transparent ($\tau_{\gamma\gamma} \lesssim 1$) for all redshifts at energies less than 20 GeV, which are those most relevant to the *Fermi*-LAT.[1].

We are grateful to the anonymous referee for useful comments which have improved this work, including the discovery of an error in the original version of Fig. 5. We thank P. Eggleton and C. Tout for correspondence regarding corrections to their stellar formulae, and A. Franceschini, R. Gilmore, and T. Kneiske for correspondence related to their EBL models. This work was supported by the Office of Naval Research and GLAST Science Investigation DPR-S-1563-Y, and by NASA Swift Guest Investigator Grant DPR-NNG05ED41I.

[1] The results of our EBL energy density and opacity calculations for use in the study of extragalactic γ-ray sources are available in electronic form by requests to the authors.

REFERENCES

Abdo, A. A. et al. 2009a, ApJ, 706, L138
—. 2009b, Science, 323, 1688
Acciari, V. A. et al. 2009, ApJ, 693, L104
Aharonian, F. et al. 2003a, A&A, 406, L9
—. 2003b, A&A, 403, 523
—. 2006, Nature, 440, 1018
—. 2007a, A&A, 470, 475
—. 2007b, A&A, 473, L25
—. 2007c, A&A, 475, L9
Albert, J. et al. 2008, Science, 320, 1752
Allen, P. D., Driver, S. P., Graham, A. W., Cameron, E., Liske, J., & de Propris, R. 2006, MNRAS, 371, 2
Babbedge, T. S. R. et al. 2006, MNRAS, 370, 1159
Baldry, I. K. & Glazebrook, K. 2003, ApJ, 593, 258
Bate, M. R. 2009, MNRAS, 392, 1363
Bernstein, R. A. 2007, ApJ, 666, 663
Bernstein, R. A., Freedman, W. L., & Madore, B. F. 2002, ApJ, 571, 56
—. 2005, ApJ, 632, 713
Blandford, R. & Eichler, D. 1987, Phys. Rep., 154, 1
Blanton, M. R. et al. 2003, ApJ, 592, 819
Böttcher, M., Dermer, C. D., & Finke, J. D. 2008, ApJ, 679, L9
Brown, R. W., Mikaelian, K. O., & Gould, R. J. 1973, Astrophys. Lett., 14, 203
Bruzual, G. & Charlot, S. 2003, MNRAS, 344, 1000
Budavári, T. et al. 2005, ApJ, 619, L31
Cambrésy, L., Reach, W. T., Beichman, C. A., & Jarrett, T. H. 2001, ApJ, 555, 563
Caputi, K. I., Lagache, G., Yan, L., Dole, H., Bavouzet, N., Le Floc'h, E., Choi, P. I., Helou, G., & Reddy, N. 2007, ApJ, 660, 97
Cirasuolo, M. et al. 2007, MNRAS, 380, 585
Cole, S. et al. 2001, MNRAS, 326, 255
Dahlen, T., Mobasher, B., Dickinson, M., Ferguson, H. C., Giavalisco, M., Kretchmer, C., & Ravindranath, S. 2007, ApJ, 654, 172
Desert, F.-X., Boulanger, F., & Puget, J. L. 1990, A&A, 237, 215
Dole, H., Lagache, G., Puget, J.-L., Caputi, K. I., Fernández-Conde, N., Le Floc'h, E., Papovich, C., Pérez-González, P. G., Rieke, G. H., & Blaylock, M. 2006, A&A, 451, 417
Driver, S. P., Popescu, C. C., Tuffs, R. J., Graham, A. W., Liske, J., & Baldry, I. 2008, ApJ, 678, L101
Dwek, E. & Arendt, R. G. 1998, ApJ, 508, L9
Dwek, E. et al. 1997, ApJ, 475, 565
—. 1998, ApJ, 508, 106
Eggleton, P. P., Fitchett, M. J., & Tout, C. A. 1990, ApJ, 354, 387
Eggleton, P. P., Tout, C. A., & Fitchett, M. J. 1989, ApJ, 347, 998
Fardal, M. A., Katz, N., Weinberg, D. H., & Davé, R. 2007, MNRAS, 379, 985
Faucher-Giguère, C.-A., Lidz, A., Hernquist, L., & Zaldarriaga, M. 2008a, ApJ, 682, L9
—. 2008b, ApJ, 688, 85
Fazio, G. G. & Stecker, F. W. 1970, Nature, 226, 135
Fazio, G. G. et al. 2004, ApJS, 154, 39
Finke, J. D. & Razzaque, S. 2009, ApJ, 698, 1761
Finke, J. D., Shields, J. C., Böttcher, M., & Basu, S. 2008, A&A, 477, 513
Fixsen, D. J., Dwek, E., Mather, J. C., Bennett, C. L., & Shafer, R. A. 1998, ApJ, 508, 123
Flores, H., Hammer, F., Thuan, T. X., Césarsky, C., Desert, F. X., Omont, A., Lilly, S. J., Eales, S., Crampton, D., & Le Fèvre, O. 1999, ApJ, 517, 148
Franceschini, A., Rodighiero, G., & Vaccari, M. 2008, A&A, 487, 837
Georganopoulos, M., Sambruna, R. M., Kazanas, D., Cillis, A. N., Cheung, C. C., Perlman, E. S., Blundell, K. M., & Davis, D. S. 2008, ApJ, 686, L5
Gilmore, R. C., Madau, P., Primack, J. R., & Somerville, R. S. 2008, in American Institute of Physics Conference Series, Vol. 1085, American Institute of Physics Conference Series, 577–580

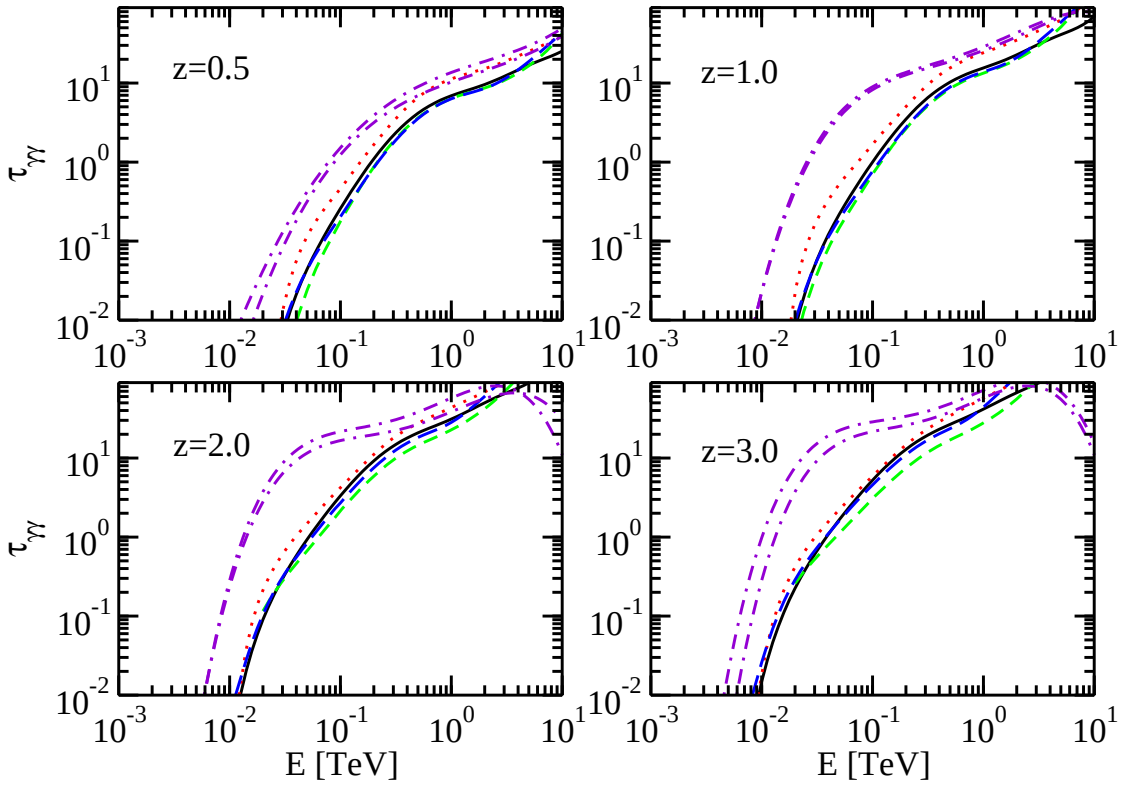

FIG. 10.— Absorption optical depth calculation for several EBL models. Curves signify the same models as in Fig. 7.

Gilmore, R. C., Madau, P., Primack, J. R., Somerville, R. S., & Haardt, F. 2009, MNRAS, 399, 1694
Gorjian, V., Wright, E. L., & Chary, R. R. 2000, ApJ, 536, 550
Gould, R. J. & Schréder, G. P. 1967, Physical Review, 155, 1404
Hauser, M. G. & Dwek, E. 2001, ARA&A, 39, 249
Hauser, M. G. et al. 1998, ApJ, 508, 25
Hopkins, A. M. & Beacom, J. F. 2006, ApJ, 651, 142
Horiuchi, S., Beacom, J. F., & Dwek, E. 2008, Phys. Rev. D, submitted, arXiv:0812.3157
Hoversten, E. A. & Glazebrook, K. 2008, ApJ, 675, 163
Huang, J.-S. et al. 2007, ApJ, 664, 840
Hurley, J. R., Pols, O. R., & Tout, C. A. 2000, MNRAS, 315, 543
Kneiske, T. M., Bretz, T., Mannheim, K., & Hartmann, D. H. 2004, A&A, 413, 807
Kneiske, T. M., Mannheim, K., & Hartmann, D. H. 2002, A&A, 386, 1
Kochanek, C. S., Pahre, M. A., Falco, E. E., Huchra, J. P., Mader, J., Jarrett, T. H., Chester, T., Cutri, R., & Schneider, S. E. 2001, ApJ, 560, 566
Krennrich, F., Dwek, E., & Imran, A. 2008, ApJ, 689, L93
Lagache, G., Dole, H., & Puget, J.-L. 2003, MNRAS, 338, 555
Le Floc'h, E. et al. 2005, ApJ, 632, 169
Levenson, L. R. & Wright, E. L. 2008, ApJ, 683, 585
Levenson, L. R., Wright, E. L., & Johnson, B. D. 2007, ApJ, 666, 34
Lien, A. & Fields, B. D. 2009, Journal of Cosmology and Astro-Particle Physics, 1, 47
Madau, P. & Pozzetti, L. 2000, MNRAS, 312, L9
Magnelli, B., Elbaz, D., Chary, R. R., Dickinson, M., Le Borgne, D., Frayer, D. T., & Willmer, C. N. A. 2009, A&A, 496, 57
Malkan, M. A. & Stecker, F. W. 1998, ApJ, 496, 13
—. 2001, ApJ, 555, 641
Marsden, G. et al. 2009, ApJ, in press, arXiv:0904.1205
Mattila, K. 2003, ApJ, 591, 119
Mazin, D. & Raue, M. 2007, A&A, 471, 439
Metcalfe, L. et al. 2003, A&A, 407, 791
Meurer, G. R. et al. 2009, ApJ, 695, 765
Nagamine, K., Ostriker, J. P., Fukugita, M., & Cen, R. 2006, ApJ, 653, 881
Papovich, C. et al. 2004, ApJS, 154, 70
Pérez-González, P. G. et al. 2005, ApJ, 630, 82
Popescu, C. C. & Tuffs, R. J. 2009, in EAS Publications Series, Vol. 34, EAS Publications Series, 247–256
Primack, J. R., Bullock, J. S., & Somerville, R. S. 2005, in American Institute of Physics Conference Series, Vol. 745, High Energy Gamma-Ray Astronomy, ed. F. A. Aharonian, H. J. Völk, & D. Horns, 23–33
Primack, J. R., Bullock, J. S., Somerville, R. S., & MacMinn, D. 1999, Astroparticle Physics, 11, 93
Primack, J. R., Gilmore, R. C., & Somerville, R. S. 2008, in American Institute of Physics Conference Series, Vol. 1085, American Institute of Physics Conference Series, 71–82
Primack, J. R., Somerville, R. S., Bullock, J. S., & Devriendt, J. E. G. 2001, in American Institute of Physics Conference Series, Vol. 558, American Institute of Physics Conference Series, ed. F. A. Aharonian & H. J. Völk, 463–+
Puget, J. L., Stecker, F. W., & Bredekamp, J. H. 1976, ApJ, 205, 638
Razzaque, S., Dermer, C. D., & Finke, J. D. 2009, ApJ, 697, 483
Reddy, N. A., Steidel, C. C., Pettini, M., Adelberger, K. L., Shapley, A. E., Erb, D. K., & Dickinson, M. 2008, ApJS, 175, 48
Salamon, M. H. & Stecker, F. W. 1998, ApJ, 493, 547
Salpeter, E. E. 1955, ApJ, 121, 161
Sandage, A., Tammann, G. A., & Yahil, A. 1979, ApJ, 232, 352
Sawicki, M. & Thompson, D. 2006, ApJ, 648, 299
Schechter, P. 1976, ApJ, 203, 297
Schroedter, M. et al. 2005, ApJ, 634, 947

Smith, A. J., Loveday, J., & Cross, N. J. G. 2008, MNRAS, submitted, arXiv:0806.0343
Stanev, T. 2004, Physics Letters B, 595, 50
Stanev, T. & Franceschini, A. 1998, ApJ, 494, L159+
Stecker, F. W., Baring, M. G., & Summerlin, E. J. 2007, ApJ, 667, L29
Stecker, F. W. & de Jager, O. C. 1993, ApJ, 415, L71+
Stecker, F. W., Malkan, M. A., & Scully, S. T. 2006, ApJ, 648, 774
Stecker, F. W. & Scully, S. T. 2008, A&A, 478, L1
Takeuchi, T. T., Ishii, T. T., Dole, H., Dennefeld, M., Lagache, G., & Puget, J.-L. 2006, A&A, 448, 525
Totani, T., Yoshii, Y., Iwamuro, F., Maihara, T., & Motohara, K. 2001, ApJ, 550, L137
Tresse, L. et al. 2007, A&A, 472, 403
Wright, E. L. & Reese, E. D. 2000, ApJ, 545, 43